THE EUROPEAN
PHYSICAL JOURNAL C

Regular Article - Theoretical Physics

Scalar and tensor resonances in J/ψ radiative decays

A. Rodas[1,2,a] , **A. Pilloni**[3,4,5,b] , **M. Albaladejo**[6], **C. Fernández-Ramírez**[7], **V. Mathieu**[8,9], **A. P. Szczepaniak**[2,10,11],
Joint Physics Analysis Center

[1] Department of Physics, College of William and Mary, Williamsburg, VA 23187, USA
[2] Theory Center, Thomas Jefferson National Accelerator Facility, Newport News, VA 23606, USA
[3] INFN Sezione di Roma, 00185 Rome, Italy
[4] Dipartimento di Scienze Matematiche e Informatiche, Scienze Fisiche e Scienze della Terra, Università degli Studi di Messina, 98166 Messina, Italy
[5] INFN Sezione di Catania, 95123 Catania, Italy
[6] Instituto de Física Corpuscular (IFIC), Centro Mixto CSIC-Universidad de Valencia, Institutos de Investigación de Paterna, Aptd. 22085, 46071 Valencia, Spain
[7] Instituto de Ciencias Nucleares, Universidad Nacional Autónoma de México, 04510 Ciudad de México, Mexico
[8] Departament de Física Quàntica i Astrofísica and Institut de Ciències del Cosmos, Universitat de Barcelona, E08028 Barcelona, Spain
[9] Departamento de Física Teórica, Universidad Complutense de Madrid and IPARCOS, 28040 Madrid, Spain
[10] Physics Department, Indiana University, Bloomington, IN 47405, USA
[11] Center for Exploration of Energy and Matter, Indiana University, Bloomington, IN 47403, USA

Abstract We perform a systematic analysis of the $J/\psi \to \gamma\pi^0\pi^0$ and $\to \gamma K_S^0 K_S^0$ partial waves measured by BESIII. We use a large set of amplitude parametrizations to reduce the model bias. We determine the physical properties of seven scalar and tensor resonances in the 1–2.5 GeV mass range. These include the well known $f_0(1500)$ and $f_0(1710)$, that are considered to be the primary glueball candidates. The hierarchy of resonance couplings determined from this analysis favors the latter as the one with the largest glueball component.

1 Introduction

The vast majority of observed mesons can be understood as simple $q\bar{q}$ bound states, although in principle strong interactions permit a more complex spectrum. In a pure Yang–Mills theory, massive gluon bound states (named "glueballs") populate the spectrum, as shown for example in lattice calculations. The lightest glueball is expected to have $J^{PC} = 0^{++}$, and a mass between 1.5 and 2 GeV [1–9]. An enhanced glueball production is expected in OZI–suppressed processes, i.e.

when the quarks of the initial state annihilate into gluons. For example, this is the case for central exclusive production in pp collisions (where mesons are produced by Pomeron – i.e. gluon ladder – fusion), or for J/ψ radiative decays, the $c\bar{c}$ must annihilate to gluons before hadronizing into the final state. In QCD, the mixing between glueballs and $q\bar{q}$ isoscalar mesons makes the identification of a glueball candidate challenging, both theoretically and experimentally. The simplest argument for the existence of a glueball component is the presence of a supernumerary state with respect to how many are predicted by the quark model [10–12]. It is thus of key importance to have a precise determination of the number and properties of the resonances seen in data.

The most recent edition of Particle Data Group (PDG) identifies nine isoscalar-scalar resonances. The two lightest ones, the $\sigma/f_0(500)$ and $f_0(980)$ have been extensively studied in recent years, and are by now very well established [13–19]. Quark model predicts other two scalars below 2 GeV, but the three $f_0(1370)$, $f_0(1500)$ and $f_0(1710)$ are observed. This stimulated an intense work to identify one of them as the long-sought glueball [20–27]. The existence of the $f_0(1370)$ is still debated. It seems to couple strongly to 4π [28,29], while the analyses of two-body final states led to contradictory results. While some analyses claim to find this resonance in either $\pi\pi \to K\bar{K}$ or $\eta\eta$ scattering [30–37] other analyses coming from meson-meson reactions do not find it [38–42]. The $f_0(1500)$ and $f_0(1710)$ are instead well established. They have been determined from $\pi\pi$ production from

fixed-target experiments [38–40,43], and from heavy meson decays [44–49], with the $f_0(1710)$ coupling mainly to kaon pairs [46,50,51]. Discerning which of the three is (or has the largest component of) the glueball, is an even harder task. Since photons do not couple directly to gluons, the scarce production of $f_0(1500)$ in $\gamma\gamma$ collisions suggests it may be dominantly a glueball. On the other hand, arguments based on the chiral suppression of the perturbative matrix element of a scalar glueball to a $q\bar{q}$ pair point to the $f_0(1710)$ as a better candidate. Although the argument does not necessarily hold nonperturbatively [52–54],[1] it seems to be supported by a quenched Lattice QCD calculation [5]. Moreover, a larger gluon content is suggested also by the enhanced associated production of $\eta' f_0(1710)$ in η_c decays [55].

The spectrum of scalars above 2 GeV is even more confusing. The PDG currently lists the $f_0(2020)$, $f_0(2100)$, $f_0(2200)$, and the $f_0(2330)$, but none of them is marked as well established. The first one has been recently confirmed by a reanalysis of the $B_s^0 \rightarrow J/\psi \pi\pi$ and $\rightarrow J/\psi K\bar{K}$ decays [49]. The $f_0(2100)$ and $f_0(2200)$ appear to decay to only pions or kaons, respectively. Since their resonance parameters are not dramatically different, they might originate from a single physical resonance (cf. Ref. [56]). Finally, the $f_0(2330)$ was seen in $p\bar{p}$ annihilations fifteen years ago [57,58], and was recently confirmed by a global reanalysis of reactions where isoscalar-scalar mesons appear [59]. The idea of characterizing the glueball properties through the couplings of all the scalar mesons to radiative J/ψ decays was considered in [59,60], and in [61] its singlet and octect mixing angles were studied.

The isoscalar-tensor sector appears to be better understood. The $f_2(1270)$ and $f_2'(1525)$ are identified as ordinary $u\bar{u} + d\bar{d}$ and $s\bar{s}$ mesons, respectively. Indeed, the former couples largely to $\pi\pi$, and the latter to $K\bar{K}$ [15,62,63]. Both resonances are relatively narrow and have also been extracted from lattice QCD with a high degree of accuracy [64].[2] The status of the other four resonances in the mass range up to 2 GeV, the $f_2(1810)$, $f_2(1910)$, $f_2(1950)$, and $f_2(2010)$, is not as clear. The $f_2(2010)$ was seen in final states with strangeness only, $K\bar{K}$ and $\phi\phi$, suggesting the $s\bar{s}$ assignment. The other decay predominantly to multibody channels, making their identification more complicated. Above 2 GeV, the PDG reports the $f_2(2150)$ and two more tensors, the $f_2(2300)$ and the $f_2(2340)$. It is worth noting that a 2^{++} glueball is also expected at about 2.5 GeV [6]. We summarize the status of the isoscalar-scalar and -tensor resonances in Table 1.

With more high precision data coming from present and future experiments, including multi-body final states, it is necessary to develop adequate amplitude analysis methods, in order to make further progress in the identification of resonances. For example, dispersive techniques that rely on fundamental S-matrix principles have played a key role in determining properties of the lightest scalar resonances [16–18,63,70–73]. Their application, however, has so far been limited to roughly the region below 1 GeV. At higher energies, other approaches, such as Padé approximants [74–77], Laurent-Pietarinen expansion [78], or the Schlessinger point method [79–81] have been used. However, these methods often require as input an analytic parametrization of the data. But – unlike men – not all parameterizations are created equal, and the ones that fulfill as many S-matrix principles as possible should be considered more trustworthy.

In this paper we extract the scalar and tensor resonances from the partial waves of $J/\psi \rightarrow \gamma\pi^0\pi^0$ and $\rightarrow \gamma K_S^0 K_S^0$ determined by BESIII [46,85]. We use a number of different parametrizations that satisfy unitarity and analyticity, in order to put under control large model dependencies. At the energies of interest, the number of available open channels makes the complete rigorous analysis unfeasible. We start by considering the $\pi\pi$ and $K\bar{K}$ final states only. Implementing unitarity on a subset of available channels does not affect seriously the resonant parameters, provided that resonances are sufficiently separated from each other [86]. For example, the most recent extractions of the lightest hybrid meson candidate include a different number of coupled channels [56,87], but their pole parameters are perfectly compatible. This is definitely not the case here. We find that 2-channel fits fail to reproduce some of the details of the resonant peaks and the interference patterns in the regions between nearest resonances. This can bias the pole determination. In addition to $\pi\pi$ and $K\bar{K}$, the PDG lists at least three other decay channels for these resonances, i.e. $\eta\eta$, $\eta\eta'$, 4π, with larger coupling to 4π. The channels $J/\psi \rightarrow \gamma (2\pi^+ 2\pi^-, \pi^+\pi^- 2\pi^0)$ were seen in the experiments done in the 80s [88,89] and later by BES [90]. BESIII also measured $J/\psi \rightarrow \gamma\eta\eta$ [44]. However, these analyses do not provide mass-independent partial wave extractions and are not comparable in statistics and quality with the most recent ones that we use. For this reason, we decided to add an effective third channel, which without loss of generality we may interpret as $\rho\rho$, but not constrained by any other data. Finally, the statistical uncertainties are determined via bootstrap [91–93].

The rest of the paper is organized as follows. A brief description of the data and our selection of the fit region is discussed in Sect. 2. We describe our set of parametrizations in Sect. 3. The 2-channel fits are described in Sects. 4, and in 5 we study the role of the third channel and perform the statistical analysis. The summary of results we obtain for

---

[1] Even perturbative arguments lead to multiple results: in Refs. [52,53] the ratios of branching ratios of the scalar glueball to $\pi\pi$ and $K\bar{K}$ is found to be proportional to $(f_\pi/f_K)^4 \simeq 0.48$.

[2] Alternative interpretations for the $f_2(1270)$ were discussed in [65–69].

Table 1 Summary of scalar and tensor resonances in the 1–2.5 GeV region listed in the PDG [84]. Resonances in square brackets are not well established. (a)Combination of entries on $\pi^+\pi^-2\pi^0$, $2\pi^+2\pi^-$, and $4\pi^0$, errors added linearly due to being asymmetric. (b)Mass and width from the $\omega\omega$ decay mode

	Mass (MeV)	Width (MeV)	$\mathcal{B}(f \to \pi\pi)$ (%)	$\mathcal{B}(f \to K\bar{K})$ (%)	$\mathcal{B}(f \to 4\pi)$ (%)
$f_0(1370)$	1200–1500	300–500	< 10 [11]	35±13 [82]	> 72 [33]
$f_0(1500)$	1506±6	112±9	34.5±2.2	8.5±1.0	48.9±3.3
$f_0(1710)$	1704±12	123±18	$3.9^{+3.0}_{-2.4}$ [83]	36±12 [26]	–
$[f_0(2020)]$	1992±16	442±60	–	–	–
$[f_0(2100)]$	2086^{20}_{-24}	284^{60}_{-32}	–	–	–
$[f_0(2200)]$	2187±14	207±40	–	–	–
$[f_0(2330)]$	2324±35	195±71	–	–	–
$f_2(1270)$	1275.5±0.8	$186.7^{+2.2}_{-2.5}$	$84.2^{+2.9}_{-0.9}$	$4.6^{+0.5}_{-0.4}$	$10.4^{+1.6}_{-3.7}$ (a)
$[f_2(1430)]$	≈ 1430	–	–	–	–
$f_2'(1525)$	1517.4±2.5	86±5	0.83±0.16	87.6±2.2	–
$[f_2(1565)]$	1542±19	122±13	–	–	–
$[f_2(1640)]$	1639±6	99^{+60}_{-40}	–	–	–
$[f_2(1810)]$	1815±12	197±22	21^{+2}_{-3} [83]	$2 \times 0.3^{+1.9}_{-0.2}$ [83]	–
$[f_2(1910)]$	1900±9 (b)	167±21 (b)	–	–	–
$f_2(1950)$	1936±12	464±24	–	–	–
$f_2(2010)$	2011^{+62}_{-76}	202^{+67}_{-62}	–	–	–
$[f_2(2150)]$	2157±12	152±30	–	–	–
$[f_2(2300)]$	2297±28	149±41	–	–	–
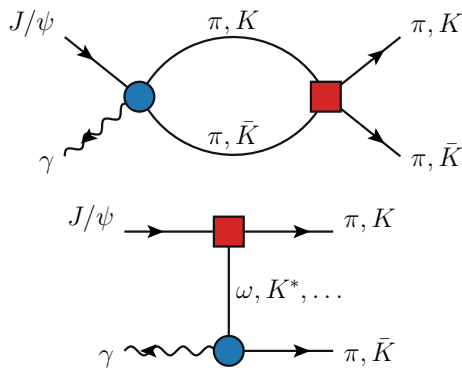
Fig. 1 Processes contributing to $J/\psi \to \gamma h\bar{h}$, with $h = \pi, K$. Top panel: J/ψ decays through short-range $c\bar{c} \to \gamma gg$ (blue disk), then resonances are seen emerging from final state interaction (red square). Bottom panel: J/ψ decays to $V h$ through the short-range $c\bar{c} \to ggg$ (red square), then the resonance V decays radiatively to $\gamma\bar{h}$ (blue disk)

the resonant poles is detailed in Sect. 6 and our conclusions are given in Sect. 7.

2 The dataset

We consider the data from the mass-independent analysis of J/ψ radiative decays, $J/\psi \to \gamma\pi^0\pi^0$ [85] and $\to \gamma K_S^0 K_S^0$ [46] by BESIII. Bose symmetry requires the two pseu-

doscalars to have $J^{PC} = (\text{even})^{++}$; moreover the isospin zero amplitude is dominant.[3] The mass independent $J = 0$ and $J = 2$ partial waves are given in the multipole basis [94]. The latter is visible in three different multipoles, $E1$, $M2$, and $E3$.[4] The three intensities look very similar up to the overall normalization with, $E1 > M2 > E3$. Considering that the quark model predicts each multipole to scale as $(E_\gamma)^{j_\gamma}$, E_γ being the photon energy, the observed hierarchy is consistent with theoretical expectation, at least close to threshold. Intensities and phase differences determined with respect to the $2^{++} E1$ are given in 15 MeV invariant mass bins, from threshold up to 3 GeV. In order to make use of the information on the relative phase, we should analyze simultaneously the S- and all the D-waves, however, because of the dominance of the lowest multipoles, we focus on 0^{++} and $2^{++} E1$.

---

[3] In fact, for the $\pi^0\pi^0$ system, isospin one is forbidden, and the decay into isospin two would be higher order in the isospin breaking. Since $I = 2$ has no resonances, there would be no dynamical mechanism that could enhance it. For the $K_S^0 K_S^0$ system, isospin one is allowed and exhibits a rich resonant structure, that includes, for example, the $a_0(980)$ and the $a_2(1320)$. However, the production of isovector is OZI-suppressed, since the topology $c\bar{c} \to \gamma gg$ couples to isoscalars only.

[4] We use the standard notation, Xj_γ, in which $j_\gamma \geq 1$ is the angular momentum carried by the electromagnetic field, and $X = E$ ($X = M$) if the parities of initial and final state satisfy (or not) $P_{\text{in}}P_{\text{fin}} = (-)^{j_\gamma}$. The values allowed for j_γ are $|J_\psi - J| \leq j_\gamma \leq J_\psi + J$.

Table 2 Branching ratios of resonances appearing in the $\gamma\bar{h}$ channel, compared to the total branching ratio. The largest contribution is given by the ω. However, it is removed in [85] by vetoing the events within 50 MeV from the nominal ω mass

$\mathcal{B}(J/\psi \rightarrow \gamma\pi^0\pi^0)$	$(11.5\pm0.5) \times 10^{-4}$	[85]
$\mathcal{B}(J/\psi \rightarrow \omega\pi^0 \rightarrow \gamma\pi^0\pi^0)$	$(3.8\pm0.4) \times 10^{-5}$	[84]
$\mathcal{B}(J/\psi \rightarrow \rho\pi^0 \rightarrow \gamma\pi^0\pi^0)$	$(2.6\pm0.5) \times 10^{-6}$	
$\mathcal{B}(J/\psi \rightarrow b_1(1232)\pi^0 \rightarrow \gamma\pi^0\pi^0)$	$(3.6\pm1.3) \times 10^{-6}$	
$\mathcal{B}(J/\psi \rightarrow \gamma K_S^0 K_S^0)$	$(8.1\pm0.4) \times 10^{-4}$	[46]
$\mathcal{B}(J/\psi \rightarrow K^*(892)^0 K_S^0 \rightarrow \gamma K_S^0 K_S^0)$	$(6.3\pm0.6) \times 10^{-6}$	[46]
$\mathcal{B}(J/\psi \rightarrow K_1(1270)^0 K_S^0 \rightarrow \gamma K_S^0 K_S^0)$	$(8.5\pm2.5) \times 10^{-7}$	
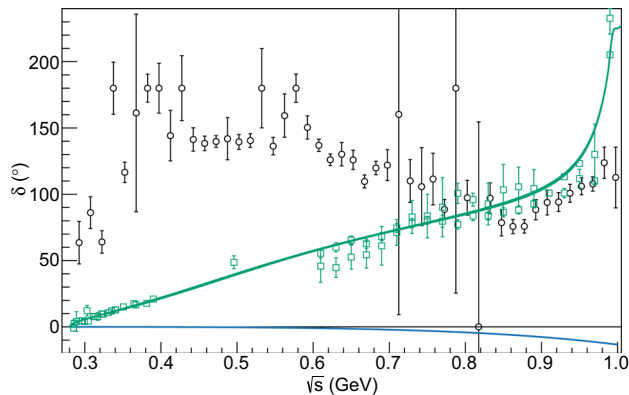
Fig. 2 S-wave $\pi\pi$ phase shifts in the elastic region. Black empty circles show the $0^{++} - 2^{++}$ $E1$ phase difference of the radiative $J/\psi \rightarrow \gamma\pi\pi$ decays by BESIII [85]. The well-known $\pi\pi$ scattering data is shown in green empty squares [36,38–40,95,96]. The dispersive fits of [15,97] are shown in green for the S-wave, and blue for (minus) the D-wave phase shift, which is basically zero at these energies. Radiative data are incompatible with the dispersive result by more than $\sim 9\sigma$, which reduce to $\sim 7\sigma$ if one allows for a constant shift

The dynamics underlying these radiative decays can be represented by the diagrams in Fig. 1. In the left diagram, the J/ψ decay is mediated by the short-range process, for example $c\bar{c} \rightarrow \gamma gg$, and resonances originate from rescattering of the two mesons. On the right diagram, the J/ψ decays through another short-range process, $e.g.$ $c\bar{c} \rightarrow ggg$ to a state containing an intermediate resonance V and a bachelor meson, $h = \pi, K$. The resonance V then decays radiatively to $\gamma\bar{h}$.[5] The latter class of reactions introduces a nontrivial background to the processes we are interested in. These intermediate resonances appear as peaks in the $\gamma\bar{h}$ invariant mass, but their contribution is mostly flat when projected onto the $h\bar{h}$ direction. Moreover, the region within 50 MeV from the dominant exchange of the ω, that appears as a narrow peak in the $\gamma\bar{h}$ Dalitz plot has been removed from the $\pi^0\pi^0$ dataset [85]. The effect of $K^*(892)$ and $K_1(1270)$ on the $K_S^0 K_S^0$ spectrum was estimated to be negligible [46]. Indeed, looking at the branching ratios given in Table 2, one can appreciate how small the contribution of these resonances is, even more so when spread over the two-meson invariant mass.

While in principle these resonances can still affect the partial waves through 3-body rescattering [98–100], it is expected that these corrections are small for large phase spaces like the ones considered here. We thus restrict the dynamics of the right diagram of Fig. 1 to possible heavier resonances that lie outside of the Dalitz plot region. The first consequence is that it is expected that Watson's theorem holds from $\pi\pi$ to $K\bar{K}$ threshold [101]. Specifically, the phase of the 0^{++} $E1$ multipole of $J/\psi \rightarrow \gamma\pi\pi$ should match that of the S-wave elastic $\pi\pi$ scattering. The latter is well established [13–16,36,38–40,95–97] and Fig. 2 compares the two. Even if one reconsidered the effect of 3-body rescattering, it would be impossible for crossed channel resonances to produce such a fast phase motion, in particular close to the $\pi\pi$ threshold. Since the focus of this work is on the higher resonances, we shall not consider further the data below the $K\bar{K}$ threshold. Moreover, no significant structure appears in data above 2.5 GeV. Since the high energy region would require a different approach [102], we also drop it from this analysis.

The extraction of partial waves from data suffers from Barrelet ambiguities [103]. For $J/\psi \rightarrow \gamma h\bar{h}$ truncated to $J = 2$, there are two possible solutions in each channel, as shown in Appendix A. While the nominal ones have a roughly vanishing 2^{++} $E1 - 2^{++}$ $M2$ phase difference, the alternative solutions display rapid motion, in particular at ~ 1.5 GeV. It is well known that the $f_2(1270)$ and $f_2'(1525)$ are mostly elastic and dominate the $\pi\pi$ and $K\bar{K}$ channels, respectively. Inelasticities contribute to $\lesssim 15\%$ to the width of each resonance. In this case, Watson's theorem requires that the phase difference between two 2^{++} multipoles vanishes in this region. Hence, the phase motions observed in the alternative solutions are not justified. These solutions also exhibit phase motion at both low and high masses, where no resonances are expected to contribute. Incidentally, the mass-dependent fit of $K\bar{K}$ in [46] clearly favors the nominal solution. For these reasons, in our analysis, we consider the nominal solutions only.

To summarize, we will perform a coupled-channel analysis of the 0^{++} $E1$ and 2^{++} $E1$ intensities and relative phase in the invariant mass region between 1 and 2.5 GeV using as data input the nominal solutions. In the following, we will

---

[5] Charge conjugation is understood.

refer to these two multipoles as *S*- and *D*-waves. In total, we fit 606 data points.

3 Amplitude models

We describe here the sets of models used to fit the data. We consider several possible variations, in order to perform a thorough study of the systematic uncertainties of our results. In the analysis of $\eta^{(\prime)}\pi$ COMPASS data [56], we chose one model as the nominal one and the differences with other models were quoted as systematic uncertainties. However, here the spread of the results is too large to permit this strategy, and we will simply list the results of each model without selecting a preferred one.

We parametrize the partial wave amplitudes following the coupled-channel N/D formalism [104–107],

$$a_i^J(s) = E_\gamma \, p_i^J \sum_k n_k^J(s) \left[D^J(s)^{-1} \right]_{ki}, \quad (1)$$

with the index $i = h\bar{h} = \pi\pi$, $K\bar{K}$, and later $\rho\rho$; as customary, s is the $h\bar{h}$ invariant mass squared, $p_i = \sqrt{s - 4m_i^2}/2$ is the breakup momentum in the $h\bar{h}$ rest frame. One power of photon energy $E_\gamma = (m_{J/\psi}^2 - s)/(2\sqrt{s})$ for E1 transitions is required by gauge invariance. The intensities are calculated as $I_i^J(s) = \mathcal{N} p_i |a_i^J(s)|^2$, with $\mathcal{N}$ a normalization factor. The $n_k^J(s)$ incorporate exchange forces (*cf.* the right diagram in Fig. 1) in the production process and are smooth functions of s in the physical region. The matrix $D^J(s)$ represents the $h\bar{h} \to h\bar{h}$ final state interactions, and contains cuts only on the real axis above thresholds (right hand cuts), which are constrained by unitarity. For the numerator $n_k^J(s)$, we use an effective polynomial expansion,

$$n_k^J(s) = \sum_{n=0}^{n_{\max}} a_{k,n}^J T_n [\omega(s)], \quad (2)$$

where T_n are the Chebyshev polynomials of order n. For systematic studies, we consider three different choices of $\omega(s)$,

$$\omega(s)_{\text{pole}} = \frac{s}{s + s_0}, \quad (3a)$$

$$\omega(s)_{\text{scaled}} = 2\frac{s - s_{\min}}{s_{\max} - s_{\min}} - 1, \quad (3b)$$

$$\omega(s)_{\text{pole+scaled}} = 2\frac{\omega(s)_{\text{pole}} - \omega(s_{\min})_{\text{pole}}}{\omega(s_{\min})_{\text{pole}} - \omega(s_{\max})_{\text{pole}}} - 1, \quad (3c)$$

where $s_0 = 1 \text{ GeV}^2$ is an effective scale parameter that controls the position of the left-hand singularities in Eqs. (3a) and (3c), and reflects the short-range nature of production. Instead, Eq. (3b) has no singularity, which corresponds to

neglecting completely the right diagram in Fig. 1. Equations (3b) and (3c) exploit the orthogonality of Chebyshev polynomials in the $[-1, 1]$ interval in order to reduce correlations, being $[s_{\min}, s_{\max}] = \left[(1 \text{ GeV})^2, (2.5 \text{ GeV})^2 \right]$ the fitting region.

A customary parametrization of the denominator is given by [106]

$$D_{ki}^J(s) = \left[K^J(s)^{-1} \right]_{ki} - \frac{s}{\pi} \int_{4m_k^2}^\infty ds' \frac{\rho N_{ki}^J(s')}{s'(s' - s - i\epsilon)}, \quad (4)$$

where

$$\rho N_{ki}^J(s')_{\text{nominal}} = \delta_{ki} \frac{(2p_i)^{2J+1}}{(s' + s_L)^{J+1+\alpha}}, \quad (5a)$$

that is an effective description of the left-hand singularities in scattering controlled by the s_L parameter, which we vary between 0 and 1 GeV^2. The parameter α controls the asymptotic behavior of the integrand, and we will use $\alpha = 0, 1$ as our preferred choices. As an alternative model, we consider the projection of a cross-channel exchange of mass squared s_L,

$$\rho N_{ki}^J(s')_{Q\text{-model}} = \delta_{ki} \frac{Q_J(z_{s'})}{2p_i^2}, \quad (5b)$$

where $Q_J(z_{s'})$ is the second kind Legendre function, and $z_{s'} = 1 + s_L/2p_i^2$. This function behaves asymptotically as $\log(s')/s'$, and has a left-hand cut starting at $s' = 4m_i^2 - s_L$. For the K-matrix, we consider

$$K_{ki}^J(s)_{\text{nominal}} = \sum_R \frac{g_k^{J,R} g_i^{J,R}}{m_R^2 - s} + c_{ki}^J + d_{ki}^J s, \quad (6a)$$

with $c_{ki}^J = c_{ik}^J$ and $d_{ki}^J = d_{ik}^J$. Alternatively, we parametrize the inverse of the S-wave K-matrix as a sum of CDD poles [86,108],

$$\left[K^J(s)^{-1} \right]_{ki}^{\text{CDD}} = c_{ki}^J - d_{ki}^J s - \sum_R \frac{g_k^{J,R} g_i^{J,R}}{m_R^2 - s}, \quad (6b)$$

where $c_{ki}^J = c_{ik}^J$ and $d_{ki}^J = d_{ik}^J$ are constrained to be positive. For a single channel, this choice ensures that no poles can appear on the first Riemann sheet. Even in the case of coupled channels, their occurrence is scarce, and when they do occur they are deep in the complex plane, far from the physical region. Ideally, the natural extension of the single-channel CDD parametrization would be the inclusion of positive defined matrices for each term in Eq. (6b). However, this is expensive to compute from a numerical point of view, and not so simple to implement in our fits [109]. No CDD-like denominator will be used for the D-wave, as its structure is much simpler. Finally, the inverse of the K-matrix could also

be parametrized as a polynomial. However, these parameterizations produce unphysical poles close to the real axis, and will not be discussed any further.
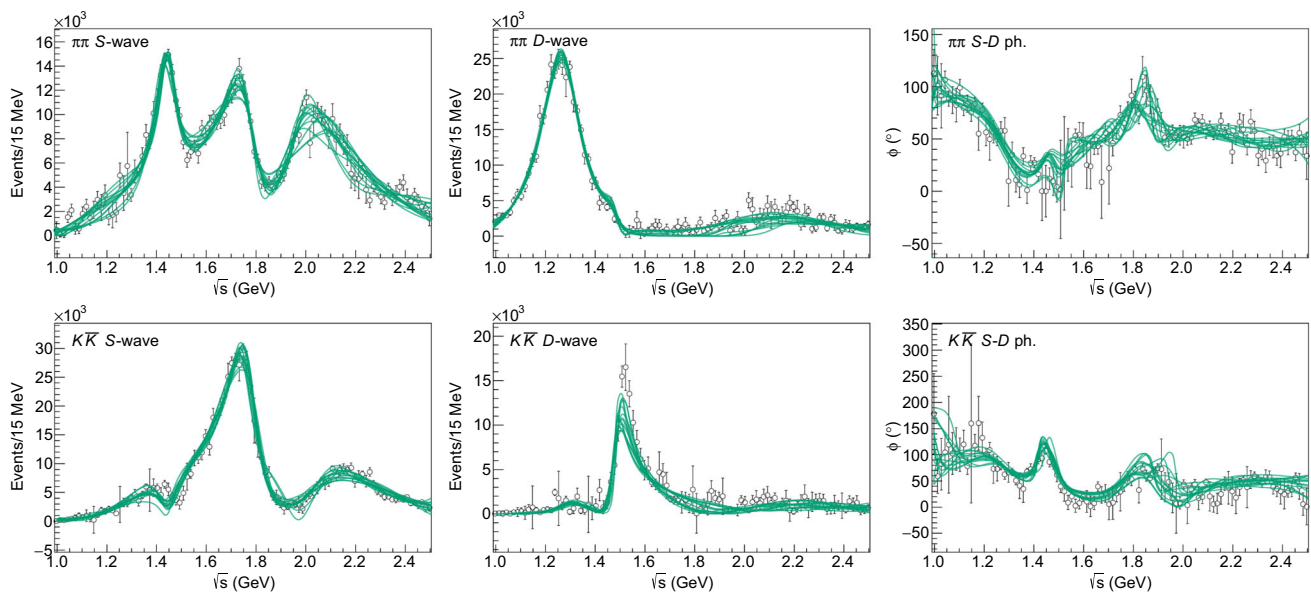
4 2-channel results

We first explore the 2-channel fits. In total, considering the various possibilities discussed in Sect. 3, we could fit 27 different amplitude choices, without considering further variations of the fixed parameters (e.g. the position of the left-hand cut, the number of K-matrix/CDD poles, the order of the polynomial in the numerator $n^J(s)$, ...), which would amount to thousands of different possibilities. For phase space functions, we consider both Eqs. (5b) and (5a) for $\alpha \leq 1$. The choice of α is motivated by the asymptotic behavior of the phase space: if $\alpha \geq 1$, the integral is oversubtracted, making other subtractions redundant. Even if those fits produce similar results and fit quality, they tend to produce narrow unphysical 1st sheet poles. Thus we restrict $\alpha = 0$ for the final best fits. For the denominator, we vary the order of the background terms. We also tried to increase the K-matrix/CDD poles from the nominal 3 to 5 to see if extra resonances are produced. These fits do not produce noticeable differences and the additional poles are unstable and far from the fitted region, effectively merging with the background. Finally, we consider the different numerator variables listed in Eq. (2). We also vary the order of the production polynomial between 2nd and 3rd order. Lower orders are not able to reproduce the data, in particular the relative phases would be heavily affected.

We select 14 models that do not produce noticeable unphysical behaviors, as 1st-sheet poles narrower than 1 GeV. Summarizing, we have 3–4 parameters per wave per channel for the numerator polynomial, 2 couplings and a mass for the six bare resonances, 3–6 per wave for the background polynomial in the denominator. Depending on the specific choices, they amount to 40–44 parameters fitted to data, by performing a χ^2 minimization with MINUIT [110].[6] For each model, the fits are initialized by randomly choosing $O(10^5)$ different sets of values for the parameters. The best fits that do not produce any unphysical behavior have $\chi^2/\text{dof} \sim 1.7$–2. We show in Fig. 3 the various 2-channel fits selected as best choices. Notice that none of them can reproduce the bump at ~ 2.4 GeV in the S-wave. Moreover, some of the dips between the peaks in the intensities are poorly described, with some local $\chi^2/\text{bins} \gtrsim 4$. As we anticipated in the Introduction, some of the resonances in the fitted region have sizeable coupling to a 4π channel, which is not

included in the two-channel fits. The absence of a channel may be responsible for producing tension between the model and the data. In particular, most of the 2-channel fits fail to describe the $f_2'(1525)$ lineshape properly, and our assumption that this state is saturated by $\pi\pi$ and $K\bar{K}$ only seems far too rigid, in particular considering that its coupling to $\pi\pi$ is negligible. This is the main reason why we expect the opening of a third channel to improve the description of data.

In these exploratory 2-channel studies no detailed statistical analysis is performed. Nevertheless, we discuss the results on the pole positions. We show in Fig. 4 the poles that appear on the Riemann sheets closest to the physical axis. Firstly, it is worth noting that not all fits produce the same number of resonant poles. Secondly, some of the fits produce additional "spurious" poles nearby, unstable upon variations of the model. As mentioned in the Introduction, the PDG lists five S- and seven D-wave resonances in this energy region, respectively (*cf.* Table 1). Grouping in clusters the poles obtained from the fits of the various models that can be identified with physical resonances is not a simple task, especially for the heavier broad resonances that have large uncertainties. Out of the 12 PDG resonances, we can identify only 6. As said, increasing the number of K-matrix/CDD poles does not help. The four lower mass clusters do not spread much and can be easily recognized. We note that the $f_0(1500)$ is lighter than what is listed in the PDG average, whereas the $f_0(1710)$ is systematically heavier. Both $f_2(1270)$ and $f_2'(1525)$ seem to have masses close to those of the PDG, although the latter's width is not very well determined in the fits. Two heavier mass clusters seem to exist, each spreading over at least two states listed in the PDG. We identify them as the $f_0(2020)$ and the $f_2(1950)$. Some models produce a fourth narrow S-wave pole at around ~ 2 GeV. One might wonder whether this cluster should be identified as the $f_0(2020)$, or as an additional state with almost the same mass. Most of the models produce the broader pole only. For those parametrizations that produce both, the narrower state has a much smaller total coupling and decays preferably to the $K\bar{K}$ state. As we will see later when including a third channel this narrow pole disappears. Finally, we note that there is no pole that could be identified with the $f_0(1370)$, even when an *ad hoc* K-matrix/CDD pole is added. However, this is not unexpected, as the $f_0(1370)$ couples mostly to 4π. Phenomenologically, little mixing is expected between this resonance and the scalar glueball [24–27], which would additionally suppress its production in J/ψ radiative decays. Its broad width would make its identification even more complicated. We conclude that, although we do not find evidence for this resonance in our analysis, its existence is not challenged. As a final remark, we note that the mass-dependent analysis of $J/\psi \to \gamma K_S^0 K_S^0$ by BESIII did find a $f_0(1370)$ with high significance [46]. We conclude that, in particular when dealing with broad resonances, the use of flexible

---

[6] This requires systematic uncertainties and correlations between partial waves to be negligible, as found in [111]. Correlations can actually be relevant, in particular in the high energy region, as shown in [102].

Fig. 3 Best 2-channel fits to $\pi\pi$ (top) and $K\bar{K}$ (second row) final states. The intensities for the S- (left), D-wave (center), and their relative phase (right) are shown. The green and red lines denote the fit results. We remark that the model variations in the 2-channel fits are much larger than the statistical uncertainties, in particular for the phases. All these fits produce $\chi^2/\mathrm{dof} \sim 1.7$–$2$

parametrizations complaint with theory constraints helps in disentangling the resonances actually required by data from background physics.

The intervals of mass and width where the six resonances appear in the best models are shown in Fig. 4 and summarized in Table 3. It is worth noting, as shown in Fig. 4, that the spreads for the heavier poles are compatible with several different resonances listed in the PDG. We remark again that we have intentionally conducted no statistical analysis here. To summarize, even though 2-channel fits describe data reasonably overall, they miss local features that affect the determination of some resonances.

5 3-Channel results

We extend our model to include a third channel corresponding to an effective 4π final state. Since we are not sensitive to the details of the dynamics populating it, we approximate it as a stable $\rho\rho$ channel, with $m_\rho = 762$ MeV [18]. Indeed, including the ρ width does not improve the fit sizably, but makes the analytic continuation extremely complicated [112].[7] Restarting the fits from scratch with an additional unconstrained channel is unfeasible. Instead, we use the best 2-channel fits of the models of Sect. 4, and use their parameters as starting point for the new 3-channel fits, to obtain more stable results. Since the 2-channel fits have reasonable

quality already, we expect the contribution of the third channel to be small. To reduce the number of parameters, the numerator coefficients $a_n^{J,\rho\rho}$ are set to zero. Moreover, in the coefficients of the background in $K^J(s)^{(-1)}$, we set the cross terms between the first two and the third channel to zero. The total number of parameters increases to 53–56, depending on the specific model.

The full list of plots and fit parameters for the 14 models is available in the Supplemental Material. In Fig. 5 we show the results for the 14 best 3-channel models. These can be compared to the 2-channel fits in Fig. 3. It is evident that the fits improve: the average χ^2/dof drops from ~ 1.7–2 to ~ 1.1–1.2. More importantly, the local description of the relative phases and of the regions around the peaks are much more accurate. The effect can be seen in Fig. 4, where it is evident that poles are determined more precisely when the new channel is added.

Most of the models lead to similar results, except for some deviation of the $K\bar{K}$ phase close to threshold. By construction our models respect Watson's theorem, which means that at the $K\bar{K}$ threshold the $\pi\pi$ and the $K\bar{K}$ phases are identical. However, in some of our fits the $K\bar{K}$ phase moves rapidly just above threshold, because of peculiar cancellations between large numerators. Another interesting feature is the "quasi-zero" behavior on the $\pi\pi$ D-wave around 1.5 GeV, which is evident in the intensity and seems to produce a sharp motion in the relative phase. A simple interpretation is that, if the D-waves are almost elastic, one expects a zero to appear between two resonances. If one assumes the coupling of the

---

[7] Alternatively, one could use approximate methods for analytic continuation, for example Padé approximants as in [49].

Table 3 Poles positions of the 2- and 3-channel fits. The intervals summarize the spread of results among the 14 best models. Statistical uncertainties are not taken into account

		$f_0(1500)$	$f_0(1710)$	$f_0(2020)$	$f_0(2330)$	$f_2(1270)$	$f_2'(1525)$	$f_2(1950)$
2-ch.	Mass (MeV)	[1420, 1456]	[1739, 1803]	[1874, 2098]	–	[1262, 1282]	[1471, 1497]	[1861, 2139]
	Width (MeV)	[70, 118]	[109, 215]	[118, 410]	–	[179, 231]	[51, 103]	[72, 320]
3-ch.	Mass (MeV)	[1437, 1471]	[1756, 1785]	[1955, 2098]	[2313, 2525]	[1256, 1279]	[1488, 1517]	[1862, 2084]
	Width (MeV)	[93, 126]	[139, 171]	[206, 427]	[180, 411]	[182, 214]	[68, 101]	[217, 539]
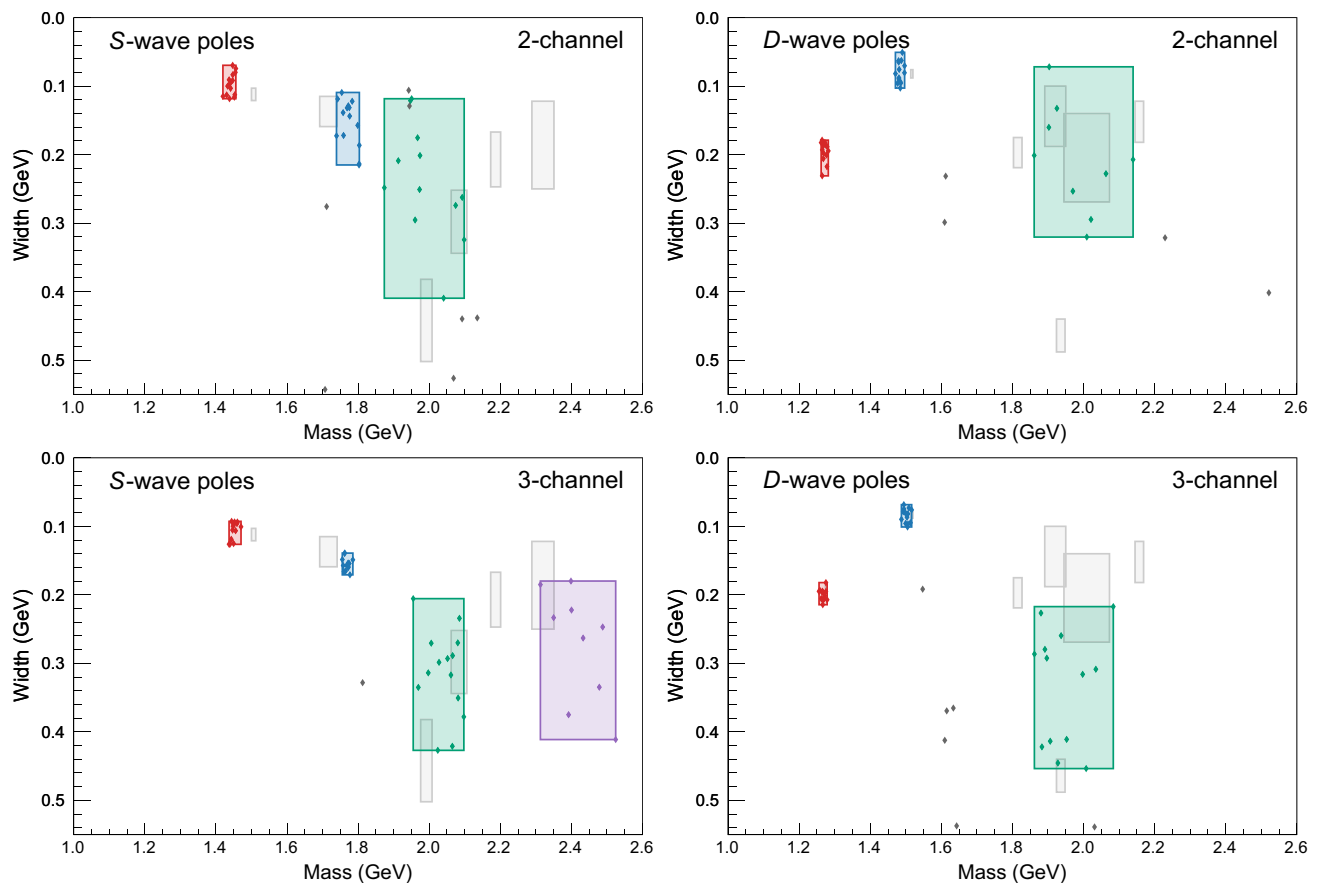
Fig. 4 Pole position of the various candidates for the 2- and 3-channel $\pi\pi$, $K\bar{K}$ fits, for the 14 systematics considered. We show in the left panels the S-wave with the $f_0(1500)$, $f_0(1710)$, $f_0(2020)$ and a possible $f_0(2330)$ resonance. In the right panels the D-wave is shown, with the $f_2(1270)$, $f_2'(1525)$ and a possible $f_2(1950)$. Identified poles are represented by colored markers, unidentified ones by gray ones. The colored rectangles represent the maximum spread in mass and width among the 14 models. For comparison, we show as gray rectangles the mass and widths (with uncertainties) of the 12 resonances listed in the PDG. We remark that the PDG lists mostly Breit-Wigner parameters, rather than pole positions in the complex plane. The 3-channel fits show a general improvement of the pole spreads. A new $f_0(2330)$ is found, while the $f_2(1950)$ is pushed deeper into the complex plane

$f_2'(1525)$ to $\pi\pi$ to be almost zero, then this behavior could be explained by the interference between the $f_2(1270)$ and a heavier resonance coupling strongly to $\pi\pi$. This matches the behavior shown in the D-wave intensity, where the $f_2(1950)$ candidate produces a small peak. Moreover, the $K\bar{K}$ D-wave does not show any rapid motion, suggesting that, were a heavy resonance to exist, it would couple mostly to the other channels.

The structure of the S-waves is much richer. There are four clearly visible peaks in $\pi\pi$, and three in $K\bar{K}$. It is worth noticing how different the values at the peak intensities look when comparing the same resonance in both final states. In particular, in $K\bar{K}$ the peak associated to the $f_0(1710)$ is roughly six times stronger than the $f_0(1500)$ one. We will show later that this is reflected in a much larger coupling of the $f_0(1710)$ to this channel. As can be seen in Fig. 5, our best
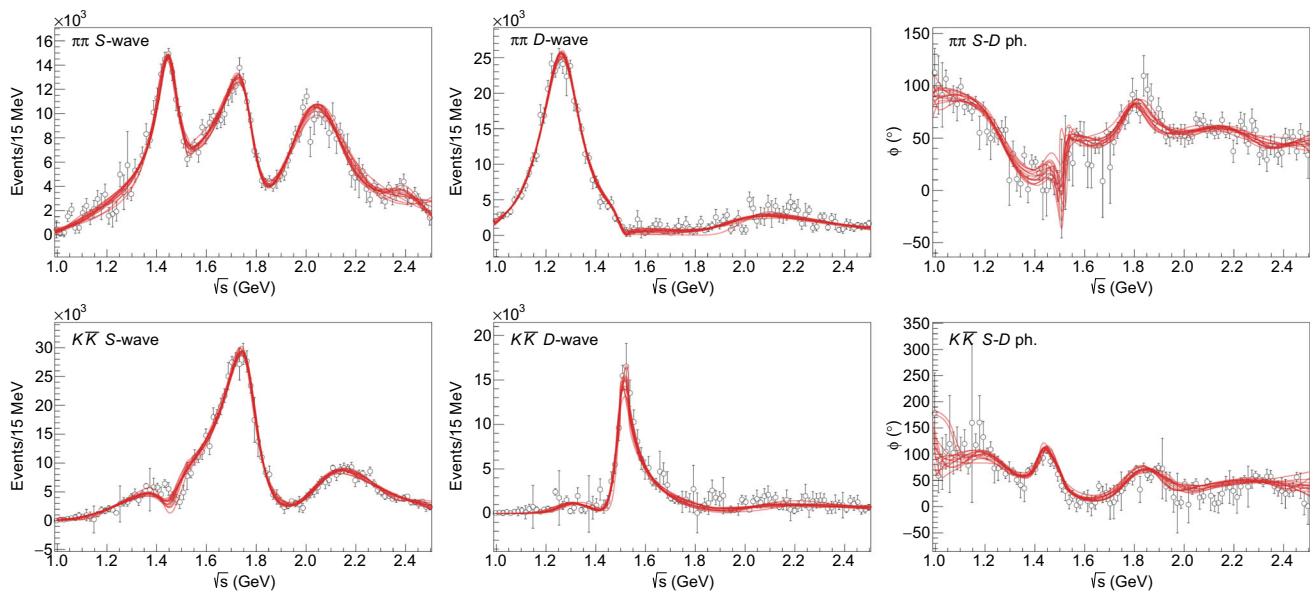
Fig. 5 Best 3-channel fits to $\pi\pi$ (top) and $K\bar{K}$ (second row) final states. The intensities for the S- (left), D-wave (center), and their relative phase (right) are shown. The red lines denote the fit results. All these produce $\chi^2/\text{dof} \sim 1.1\text{–}1.2$
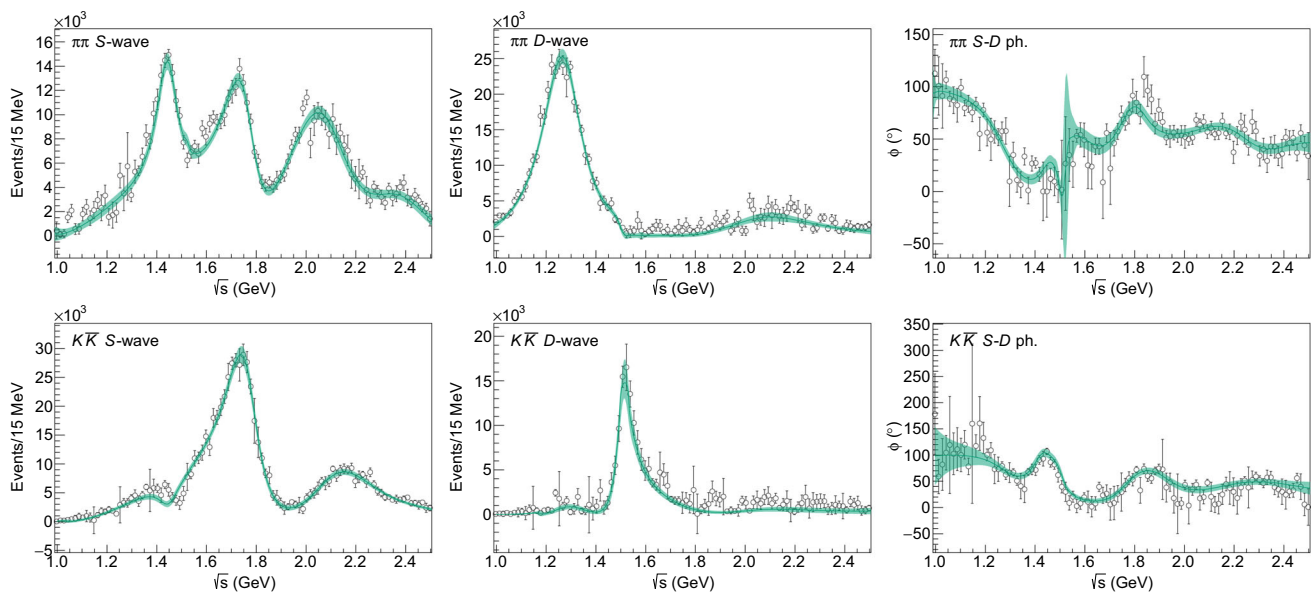
Fig. 6 One of the final 3-channel fits, with statistical uncertainties included. The solid line and green band show the central value and the 1σ confidence level provided by the bootstrap analysis, calculated for $O(10^4)$ samples

fit reproduces all intensity peaks with high accuracy. There is a slightly larger local χ^2 value around the 1.5 GeV region in the $K\bar{K}$ S-wave. This region is below the $\rho\rho$ open channel, which seems to prevent our fit from fully reproducing the peak and interference. We are aware that the $f_0(1500)$ resonance couples to 4π, but the local description is nevertheless reasonable. We thus conclude that a third channel is not strictly needed to describe such behavior. Ideally, the $\rho\rho$ channel should include both $\ell = 0$ and $\ell = 2$ contributions. However, the latter is suppressed at threshold, and

having no data to fit makes it impossible to distinguish the two. Nonetheless, we performed some alternative fits including just an $\ell = 2$ channel to assess our systematics. We get $\chi^2/\text{dof} \sim 1.4$, not as good as in the $\ell = 0$ case, being the channel suppressed as mentioned. The pole positions calculated this way are compatible with the $\ell = 0$ models (see below), and we do not see much variation in the S-wave, as expected. We do not consider these fits any further. Even for these 3-channel fits, there is no evidence for more resonances than the seven ones discussed above. Fits with additional K-

matrix/CDD poles do not improve the data description, and the additional poles are far and unstable.

The statistical uncertainties are determined via bootstrap [91–93]. We generate $O(10^4)$ pseudodatasets: each data point is resampled from a gaussian distribution having by mean and standard deviation its value and uncertainty; to avoid unphysical negative intensities, data points compatible with zero within 2σ are instead resampled from a Gamma distribution (see Appendix B). Each pseudodataset is refitted to the original model, and the (co)variance of the population of the fit parameters provides an estimate of their statistical uncertainties and correlations. In Fig. 6 we show as an example the uncertainties for one of the models.

6 Resonant poles

As already discussed, it is not possible to fix a priori the number of poles that appear on the proximal Riemann sheets. In general, there is no one-to-one correspondence between the poles of the amplitude and the number of K-matrix/CDD poles in coupled channel problems. This relation becomes even more complicated because of the additional background polynomial. Moreover, the simple left-hand cut parametrizations in $\rho N_{ki}^J(s')$ also tend to generate additional broad poles close to threshold [86]. Some of the poles capture the real features of the amplitude and are associated with the physical resonances. Other poles are mere artifacts of the model implemented and are unstable upon bootstrap and model variations. Therefore, a sound statistical analysis and a large set of systematic variations are required to filter out the spurious singularities and identify the remaining ones with the physical resonances. The pole positions for the systematic variations of amplitudes studied here are plotted in Fig. 7, while the separate plots for each systematic are left in the Supplemental Material. For each model, the statistical uncertainties are determined via bootstrap, as explained in Sect. 5. While in [56] we were able to identify a nominal model and explored how model variation affected the central values, here the clusters of poles, in particular the heavier ones, move too much
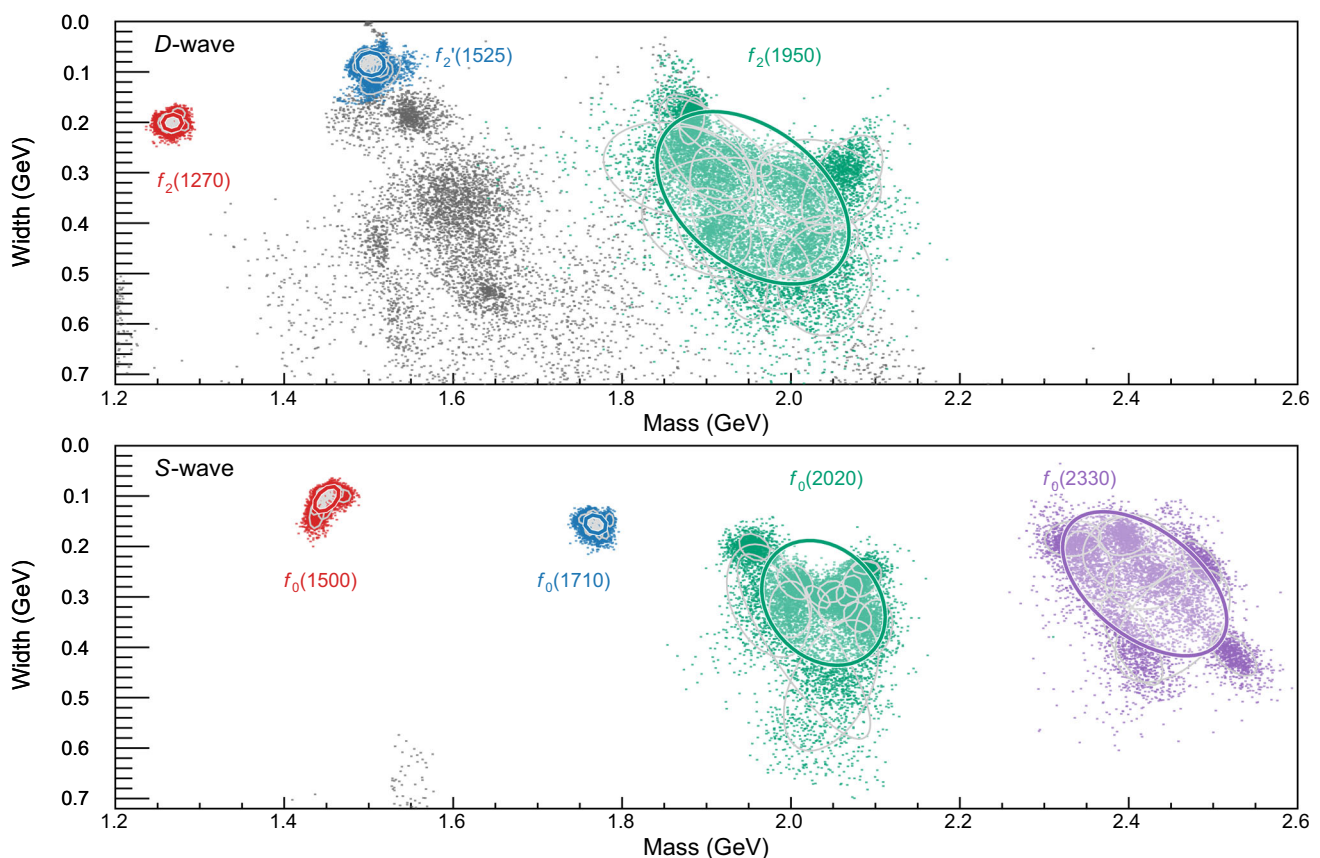
Fig. 7 Results for the pole positions of the 3-channel fits, superimposed for the 14 models. A point is drawn for each pole found in each of the $O(10^4)$ pseudodatasets generated by the bootstrap analysis. Colored points represent poles identified as a physical resonance, gray points are spurious. For the physical resonance, gray ellipses show the 68% confidence region of each systematic. Colored ellipses show the average of all 14 systematics, as explained in the text

to make this strategy feasible. In order to quote an average of masses and widths obtained by the 14 models, we calculate the mean and (co)variance of the pole positions among the $14 \times O(10^4)$ pseudodatasets from the bootstrap analysis for all the models at once.

In addition to the pole positions, one can extract the residues of the amplitude. The residues of $a_i^J(s)$ can be associated with the couplings of the resonance f to the initial $J/\psi\,\gamma$ and final $h\bar{h}$ states. We remark that we do not include all the possible open channels involved at these energies. However, since the unconstrained third $\rho\rho$ channel can effectively reabsorb the presence of other channels, we believe that the relative size of the $\pi\pi$ and $K\bar{K}$ coupling provides reliable information. One can also study the residues of the $D^J(s)^{-1}$ matrix, that are connected to the scattering couplings $h\bar{h} \to f \to h'\bar{h}'$, albeit not rigorously.[8] Since we are not fitting scattering data, the residues of $D^J(s)^{-1}$ are mostly unconstrained and have large uncertainties [113].

The lightest two D-wave poles are very well determined. They correspond to the $f_2(1270)$ and $f_2'(1525)$ resonances, and decay almost elastically to $\pi\pi$ and $K\bar{K}$ respectively. The f_2 peak in $\pi\pi$ and the f_2' peak in $K\bar{K}$ is very well described by all models. The f_2' lies close to the $\rho\rho$ threshold, so we have to ensure that the poles that form the cluster appear always on the proximal Riemann sheet. For all the models, the f_2' is always centered below this threshold. Even though we do not fit scattering data directly, these resonances are so well behaved that the scattering couplings have reasonable ratios:

$$f_2(1270): \quad r_{\pi\pi}\Big/\sqrt{r_{\pi\pi}^2 + r_{K\bar{K}}^2} = 82^{+6}_{-8}\%,$$

$$f_2'(1525): \quad r_{K\bar{K}}\Big/\sqrt{r_{\pi\pi}^2 + r_{K\bar{K}}^2} = 95^{+3}_{-5}\%, \qquad (7)$$

where $r_{h\bar{h}}$ are the absolute values of the residues of the $D^J(s)^{-1}$ matrix in the elastic $h\bar{h} \to h\bar{h}$ channel. These are reasonably close to the PDG estimates [84]. Some of the fits produce a second broader cluster in D-wave behind the $f_2'(1525)$. As can be seen in the Supplemental Material, this second pole appears in most of the K-matrix parametrizations, often with very large spread, but not in the CDD ones. Furthermore, when the pole appears the local χ^2 in that region does not improve. For these reasons, the existence of an additional resonance is not compelling in data.

Moving to the S-wave, our result for the $f_0(1500)$ is perfectly compatible with [49], even though we have a $f_0(1710)$ close by, which could easily affect its pole position. The

$f_0(1500)$ turns out to be rather narrow and produces a simple phase motion for the S-wave phases. The $f_0(1710)$ is noticeably broader, but nevertheless very well determined. The mass we find for the $f_0(1710)$ is considerably larger than the PDG average, however, it is still compatible with many of the determinations listed in the PDG. All the four scalar resonances we found are roughly compatible with those identified in [59], although what we call $f_0(1710)$ and $f_0(2020)$ seem to correspond to their $f_0(1770)$ and $f_0(2100)$.

When comparing the $f_0(1500)$ and $f_0(1710)$ couplings of the full $J/\psi \to \gamma f_0 \to \gamma h\bar{h}$ process, we find that the heavier one couples more strongly to both final states. In particular the coupling of the $f_0(1710)$ to $K\bar{K}$ is roughly eight times larger than that of the $f_0(1500)$ and roughly three times larger in $\pi\pi$, as can be seen in Fig. 8. It is worth noting that the values of the residues change substantially under ampli-
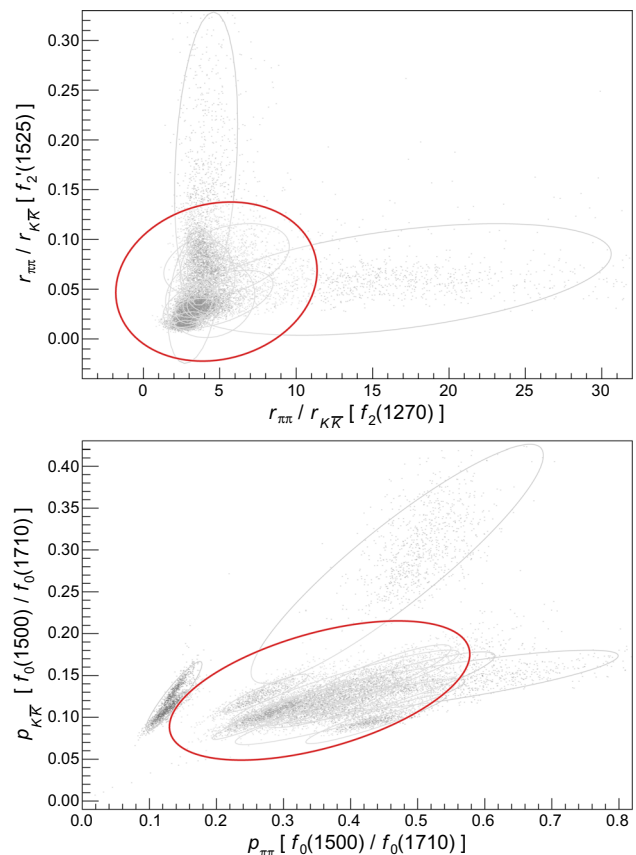
Fig. 8 Top panel: ratio of absolute values of the scattering residues of $\pi\pi$ and $K\bar{K}$ final states, for the $f_2(1270)$ against the $f_2'(1525)$. Bottom panel: ratio of absolute values of decay residues of $f_0(1500)$ and $f_0(1710)$, for $\pi\pi$ against $K\bar{K}$ final state. A point is drawn for each pole found in each of the $O(10^4)$ pseudodatasets generated by the bootstrap analysis. Gray ellipses show the 68% confidence region of each systematic. The colored ellipses represent the 68% confidence region of all the systematics at once. Ratios are nongaussian positive-defined quantities, and the results of each systematics scarcely overlap, so this ellipse cannot be taken literally, but nevertheless provides a crude idea of average values, errors, and correlations

---

[8] To get the full scattering amplitude, the $D^J(s)^{-1}$ matrix should be multiplied by the appropriate $N^J(s)$ that satisfies an integral equation that depends on the left-hand cuts of the scattering process. However, since $N^J(s)$ is smooth, we believe it should not affect much the relative size of the couplings, that we discuss here.

Table 4 List of final pole position and uncertainties resulting from the combination of the 14 different final fits to the data. The errors have been obtained as the variance of the full samples, by assuming that the spread of results for each pole, shown in Fig. 7, resembles a Gaussian distribution

S-wave	$\sqrt{s_p}$ (MeV)	D-wave	$\sqrt{s_p}$ (MeV)
$f_0(1500)$	$(1450\pm10) - i(106\pm16)/2$	$f_2(1270)$	$(1268\pm8) - i(201\pm11)/2$
$f_0(1710)$	$(1769\pm8) - i(156\pm12)/2$	$f_2(1525)$	$(1503\pm11) - i(84\pm15)/2$
$f_0(2020)$	$(2038\pm48) - i(312\pm82)/2$	$f_2(1950)$	$(1955\pm75) - i(350\pm113)/2$
$f_0(2330)$	$(2419\pm64) - i(274\pm94)/2$		

tude variations, which makes us cautious about strong claims regarding a precise determination of these ratios. However, all determinations agree qualitatively: the heavier resonance is stronger in J/ψ radiative decays, and in particular in the $K\bar{K}$ channel. As we mentioned in the Introduction, these arguments favor the interpretation for the $f_0(1710)$ to have a sizeable glueball component.

The final set of poles that can be identified as physical ones is shown in Fig. 7, and the mean values and uncertainties are listed in Table 4. It is worth noting that our poles are compatible with the ones on the BESIII $J/\psi \to \gamma\eta\eta$ decay [44], even if we do not include this channel. This supports our choice of including the most relevant high-statistics $\pi\pi$ and $K\bar{K}$ channels only.

7 Summary

We presented a detailed analysis of the isoscalar-scalar and -tensor resonances in the 1–2.5 GeV mass region. We study the BESIII mass-independent partial waves from $J/\psi \to \gamma\pi^0\pi^0$ and $\to \gamma K_S^0 K_S^0$ radiative decays [46,85]. Data were published in two equivalent solutions in the full kinematic range. However, the region below the $K\bar{K}$ threshold is not compatible with Watson's theorem expectation, which made us select one of the two solutions and restrict the fit to the 1–2.5 GeV mass region. To assess the model dependence realistically, we explored a large number of amplitude parametrizations that respect the S-matrix principles as much as possible and discuss the results for 14 of them. We first enforce unitarity strictly on the two channels considered, which turns out to be too rigid to describe data, in particular between the resonant peaks. We then extend our models to include a third unconstrained $\rho\rho$ channel, which is known to contribute substantially to the resonances in this region. Fit quality is excellent for all the parametrizations studied. Despite the large systematic uncertainties, we can identify four scalar and three tensor states.

The four lightest resonances are determined with great accuracy, which allows us to study their couplings. We find that the $f_2(1270)$ and $f_2'(1525)$ couple largely to $\pi\pi$ and $K\bar{K}$, respectively, as expected by their quark model assign-
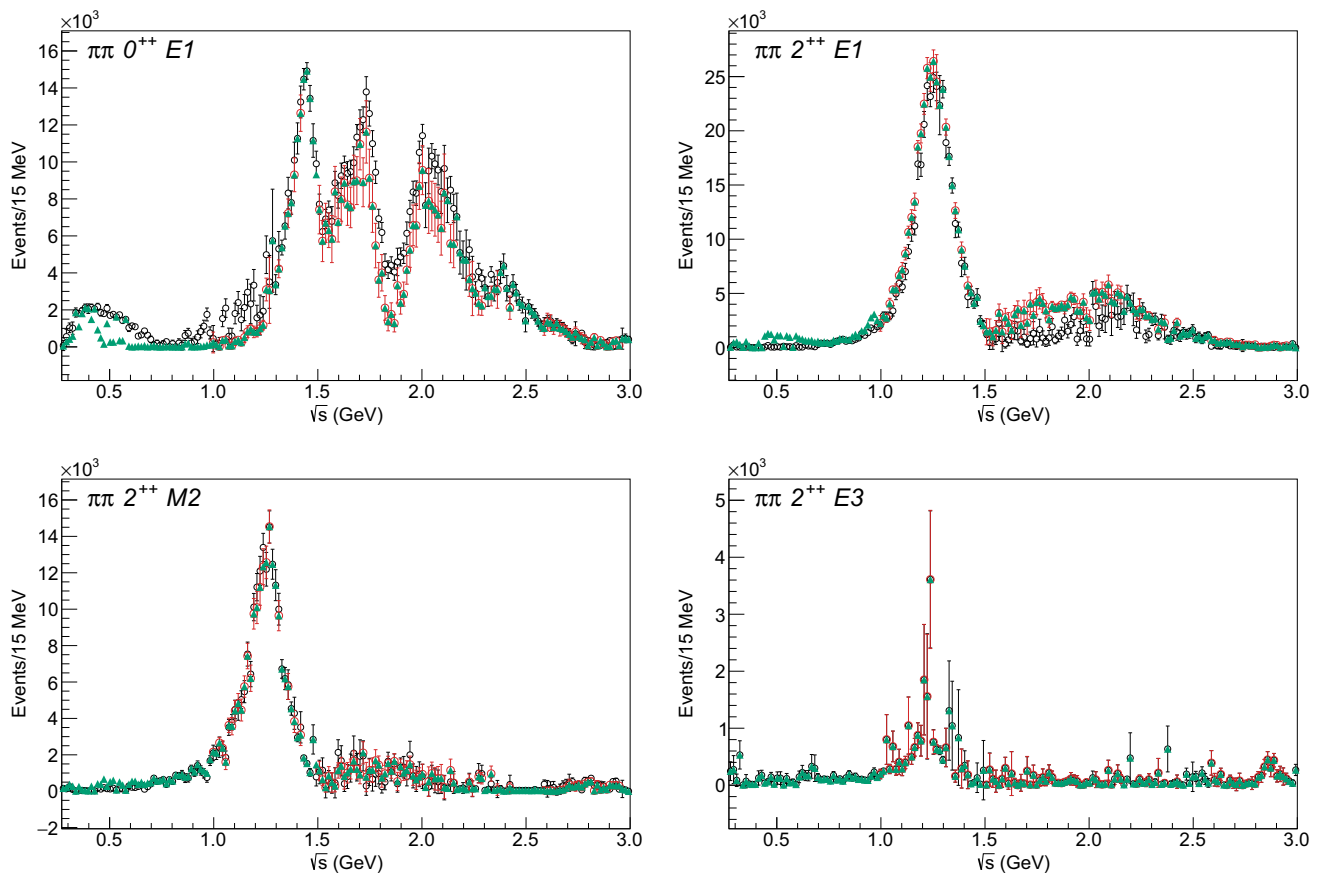
ments. The couplings ratios are compatible with the branching fractions reported in the PDG. In the scalar sector, it seems that the $f_0(1710)$ appears in $J/\psi \to \gamma f_0$ more strongly than the $f_0(1500)$. This affinity of the $f_0(1710)$ to the gluon-rich initial state, together with a coupling to $K\bar{K}$ larger by one order of magnitude, are hints for a sizeable glueball component.

Fig. 9 Comparison between the nominal (black) and ambiguous (red) solutions for the intensities extracted in [85]. The prediction for the latter is shown in green using the relations derived in the experimental paper and extended below the $K\bar{K}$ threshold

Appendix A: $J/\psi \to \gamma\pi\pi$ Ambiguities

As mentioned in Sect. 2, partial wave extractions suffer from ambiguities. Specifically, the $J/\psi \to \gamma h\bar{h}$ radiative decays truncated to the 2^{++} multipoles, can have two different solutions, related mathematically [46,85]: in a given energy bin, one can calculate the intensities and relative phases of the four multipoles of one solution from the intensities and relative phases of the four multipoles of the other solution. Below the $K\bar{K}$ threshold, the experimental papers do not show the ambiguous solution: Watson's theorem is invoked in order to discard one of them. However, as we showed in Sect. 2, Watson's theorem also implies the 0^{++} $E1$ phase to match the S-wave elastic $\pi\pi$ scattering shift, which is not the case. Based on this, and on the fact that the ambiguous solutions in $\pi\pi$ and $K\bar{K}$ shows some unexpected behaviour in the phases, we decided to focus on the nominal solution, and discard the region below 1 GeV.

Nevertheless, we tried to see whether there is a way to make use of these data in the region where the much-studied $\sigma/f_0(500)$ and the $f_0(980)$ appear. Since the existence of ambiguities is a mathematical fact that does not depend on unitarity arguments like Watson's theorem, we can calculate the ambiguous solution of $J/\psi \to \gamma\pi^0\pi^0$ below $K\bar{K}$ threshold and check whether it agrees better with $\pi\pi$ scattering. The exercise is shown in Figs. 9 and 10. Since the relative phase of the three 2^{++} multipoles is set to zero below the $K\bar{K}$ threshold, this turns into an underestimation of the errors of the ambiguous solution, which looks very scattered (in particular for the phases) and unusable.

We even tried to proceed in the opposite direction: replacing the measured 0^{++} $E1$ phase with the known S-wave elastic $\pi\pi$ scattering one, we can calculate what would its ambiguous counterpart be. The result is shown in Fig. 11. This looks closer to the BESIII phase, although with some differences, most notably the sharp rise at ~ 900 MeV.

Appendix B: Bootstrap and the Γ distribution

Bootstrapping has become in the recent past a promising method to assess uncertainties in spectroscopy analyses [56,86,93,100,102,114–116]. In particular, it allows one to map the likelihood for a given minimum, which is not accessi-
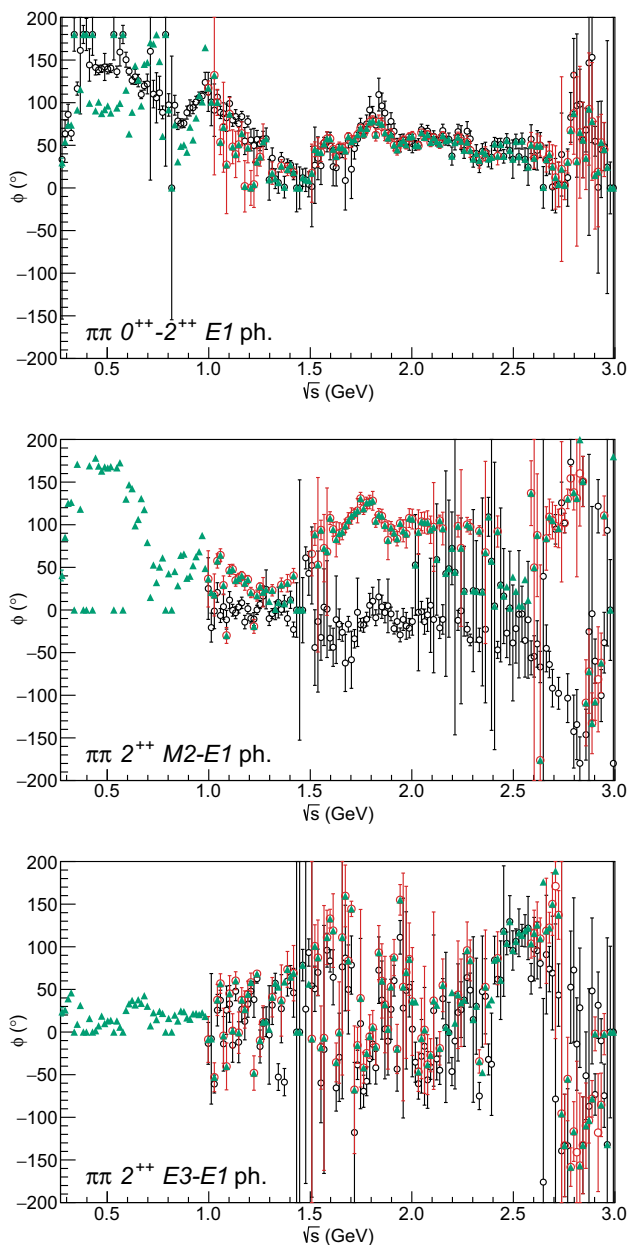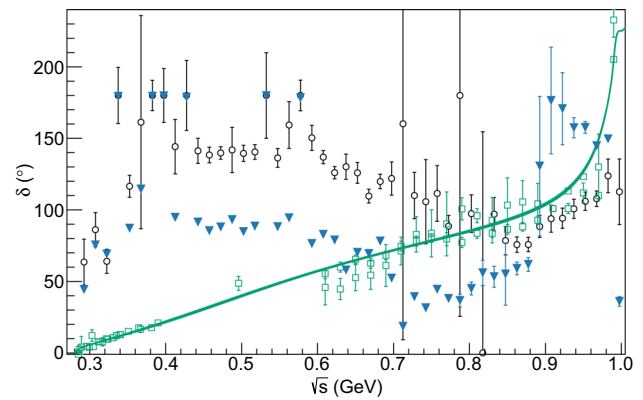
Fig. 10 Comparison between the nominal (black) and ambiguous (red) solutions for the relative phases extracted in [85]. The prediction for the latter is shown in green using the relations derived in the experimental paper, and extended below the $K\bar{K}$ threshold

Fig. 11 Comparison between the nominal BESIII data, the elastic $\pi\pi$ phase shift from [97] (solid green band) and the predicted ambiguous partner of the latter

points compatible with zero, or even negative values, within 1σ, which is not physical, and no sensible parametrization can reproduce. In this sense using a simple normal distribution to resample the data would produce artifacts in our uncertainties, which would then propagate into the pole errors.

For all intensity data points which are compatible with zero within 2σ, we assume they follow a Γ distribution, having by mean and variance the central value and the error squared. This was used in previous spectroscopy analyses [118]. The distribution is given by

$$H(x\|\mu,\sigma) = \theta(x)\left(\frac{x\mu}{\sigma^2}\right)^{\frac{\mu^2}{\sigma^2}}\frac{\exp\left(-x\mu/\sigma^2\right)}{x\,\Gamma\left(\mu^2/\sigma^2\right)}. \tag{B.1}$$

This distribution is positive defined and has light tails as the gaussian, which makes it a good candidate for our purposes. Its mean and variance are μ and σ^2, and it smoothly convergences to the gaussian distribution as the ratio μ/σ increases.

ble through simple error propagation in non-linear problems, or when the number of parameters is very large. Furthermore, this technique can also help us distinguish between stable "physical" poles and spurious ones [56,117], whereas simple error propagation would fail to describe robustly those uncertainties.

One usually assumes data points to be normally distributed. However, the intensities extracted in [46,85] are positive defined, and since they are not simple event counts, they are not even Poisson distributed. There are several data

References

1. G.S. Bali, K. Schilling, A. Hulsebos, A.C. Irving, C. Michael, P.W. Stephenson (UKQCD), Phys. Lett. B **309**, 378 (1993), https://doi.org/10.1016/0370-2693(93)90948-H. arXiv:hep-lat/9304012
2. A. Patel, R. Gupta, G. Guralnik, G.W. Kilcup, S.R. Sharpe, Phys. Rev. Lett. **57**, 1288 (1986). https://doi.org/10.1103/PhysRevLett.57.1288
3. M. Albanese et al., APE Phys. Lett. B **192**, 163 (1987). https://doi.org/10.1016/0370-2693(87)91160-9
4. C. Michael, M. Teper, Nucl. Phys. B **314**, 347 (1989). https://doi.org/10.1016/0550-3213(89)90156-9
5. J. Sexton, A. Vaccarino, D. Weingarten, Phys. Rev. Lett. **75**, 4563 (1995). https://doi.org/10.1103/PhysRevLett.75.4563 arXiv:hep-lat/9510022
6. C.J. Morningstar, M.J. Peardon, Phys. Rev. D **60**, 034509 (1999). https://doi.org/10.1103/PhysRevD.60.034509 arXiv:hep-lat/9901004
7. A.P. Szczepaniak, E.S. Swanson, Phys. Lett. B **577**, 61 (2003). https://doi.org/10.1016/j.physletb.2003.10.008 arXiv:hep-ph/0308268

8. Y. Chen et al., Phys. Rev. D **73**, 014516 (2006). arXiv:hep-lat/0510074

9. A. Athenodorou, M. Teper, JHEP **11**, 172 (2020). https://doi.org/10.1007/JHEP11(2020)172 arXiv:2007.06422 [hep-lat]

10. V. Mathieu, N. Kochelev, V. Vento, Int. J. Mod. Phys. E **18**, 1 (2009). https://doi.org/10.1142/S0218301309012124 arXiv:0810.4453 [hep-ph]

11. W. Ochs, J. Phys. G **40**, 043001 (2013). https://doi.org/10.1088/0954-3899/40/4/043001 arXiv:1301.5183 [hep-ph]

12. F.J. Llanes-Estrada, Eur. Phys. J. ST (2021). https://doi.org/10.1140/epjs/s11734-021-00143-8 arXiv:2101.05366 [hep-ph]

13. B. Ananthanarayan, G. Colangelo, J. Gasser, H. Leutwyler, Phys. Rep. **353**, 207 (2001). https://doi.org/10.1016/S0370-1573(01)00009-6 arXiv:hep-ph/0005297

14. G. Colangelo, J. Gasser, H. Leutwyler, Nucl. Phys. B **603**, 125 (2001). https://doi.org/10.1016/S0550-3213(01)00147-X arXiv:hep-ph/0103088

15. R. García-Martín, R. Kamiński, J.R. Peláez, J. Ruiz de Elvira, F.J. Ynduráin, Phys. Rev. D **83**, 074004 (2011). https://doi.org/10.1103/PhysRevD.83.074004 arXiv:1102.2183 [hep-ph]

16. B. Moussallam, Eur. Phys. J. C **71**, 1814 (2011). https://doi.org/10.1140/epjc/s10052-011-1814-z arXiv:1110.6074 [hep-ph]

17. I. Caprini, G. Colangelo, H. Leutwyler, Phys. Rev. Lett. **96**, 132001 (2006). https://doi.org/10.1103/PhysRevLett.96.132001 arXiv:hep-ph/0512364

18. R. García-Martín, R. Kaminski, J.R. Peláez, J. Ruiz de Elvira, Phys. Rev. Lett. **107**, 072001 (2011). https://doi.org/10.1103/PhysRevLett.107.072001 arXiv:1107.1635 [hep-ph]

19. J.R. Peláez, Phys. Rep. **658**, 1 (2016). https://doi.org/10.1016/j.physrep.2016.09.001 arXiv:1510.00653 [hep-ph]

20. M.S. Chanowitz, Phys. Rev. Lett. **46**, 981 (1981). https://doi.org/10.1103/PhysRevLett.46.981

21. C. Amsler, F.E. Close, Phys. Rev. D **53**, 295 (1996). https://doi.org/10.1103/PhysRevD.53.295 arXiv:hep-ph/9507326

22. C. Amsler, F.E. Close, Phys. Lett. B **353**, 385 (1995). https://doi.org/10.1016/0370-2693(95)00579-A arXiv:hep-ph/9505219

23. W.-J. Lee, D. Weingarten, Phys. Rev. D **61**, 041015 (2000). https://doi.org/10.1103/PhysRevD.61.014015 arXiv:hep-lat/9910008

24. F. Giacosa, T. Gutsche, V. Lyubovitskij, A. Faessler, Phys. Rev. D **72**, 094006 (2005). https://doi.org/10.1103/PhysRevD.72.094006 arXiv:hep-ph/0509247

25. F. Giacosa, T. Gutsche, V.E. Lyubovitskij, A. Faessler, Phys. Lett. B **622**, 277 (2005). https://doi.org/10.1016/j.physletb.2005.07.016 arXiv:hep-ph/0504033

26. M. Albaladejo, J.A. Oller, Phys. Rev. Lett. **101**, 252002 (2008). https://doi.org/10.1103/PhysRevLett.101.252002 arXiv:0801.4929 [hep-ph]

27. S. Janowski, F. Giacosa, D.H. Rischke, Phys. Rev. D **90**, 114005 (2014). https://doi.org/10.1103/PhysRevD.90.114005 arXiv:1408.4921 [hep-ph]

28. A. Abele et al., Cryst. Barrel Eur. Phys. J. C **19**, 667 (2001). https://doi.org/10.1007/s100520100601

29. A. Abele et al., Cryst. Barrel Eur. Phys. J. C **21**, 261 (2001). https://doi.org/10.1007/s100520100735

30. C. Amsler et al., Cryst. Barrel Phys. Lett. B **291**, 347 (1992). https://doi.org/10.1016/0370-2693(92)91057-G

31. V. Anisovich et al., Cryst. Ball Phys. Lett. B **323**, 233 (1994). https://doi.org/10.1016/0370-2693(94)90297-6

32. C. Amsler et al., Cryst. Barrel Phys. Lett. B **353**, 571 (1995). https://doi.org/10.1016/0370-2693(95)00610-W

33. M. Gaspero, Nucl. Phys. A **562**, 407 (1993). https://doi.org/10.1016/0375-9474(93)90206-D

34. A. Adamo et al., Nucl. Phys. A **558**, 13 (1993). https://doi.org/10.1016/0375-9474(93)90379-C

35. C. Amsler et al., Cryst. Barrel Phys. Lett. B **322**, 431 (1994). https://doi.org/10.1016/0370-2693(94)91176-2

36. D.H. Cohen, D.S. Ayres, R. Diebold, S.L. Kramer, A.J. Pawlicki, A.B. Wicklund, Phys. Rev. D **22**, 2595 (1980). https://doi.org/10.1103/PhysRevD.22.2595

37. A. Etkin et al., Phys. Rev. D **25**, 2446 (1982). https://doi.org/10.1103/PhysRevD.25.2446

38. B. Hyams et al., Nucl. Phys. B **64**, 134 (1973). https://doi.org/10.1016/0550-3213(73)90618-4

39. G. Grayer et al., Nucl. Phys. B **75**, 189 (1974). https://doi.org/10.1016/0550-3213(74)90545-8

40. B. Hyams et al., Nucl. Phys. B **100**, 205 (1975). https://doi.org/10.1016/0550-3213(75)90616-1

41. P. Estabrooks, Phys. Rev. D **19**, 2678 (1979). https://doi.org/10.1103/PhysRevD.19.2678

42. C. Adolph et al., (COMPASS), Phys. Rev. D **95**, 032004 (2017). https://doi.org/10.1103/PhysRevD.95.032004. arXiv:1509.00992 [hep-ex]

43. S. Chandavar et al., (CLAS), Phys. Rev. C **97**, 025203 (2018). https://doi.org/10.1103/PhysRevC.97.025203. arXiv:1712.02184 [nucl-ex]

44. M. Ablikim et al., BESIII. Phys. Rev. D **87**, 092009 (2013). https://doi.org/10.1103/PhysRevD.87.092009. arXiv:1301.0053 [hep-ex] [Erratum: Phys. Rev. D 87, 119901 (2013)]

45. S. Dobbs, A. Tomaradze, T. Xiao, K.K. Seth, Phys. Rev. D **91**, 052006 (2015). https://doi.org/10.1103/PhysRevD.91.052006 arXiv:1502.01686 [hep-ex]

46. M. Ablikim et al. (BESIII), Phys. Rev. D **98**, 072003 (2018). https://doi.org/10.1103/PhysRevD.98.072003. arXiv:1808.06946 [hep-ex]

47. P. d'Argent, N. Skidmore, J. Benton, J. Dalseno, E. Gersabeck, S. Harnew, P. Naik, C. Prouve, J. Rademacker, JHEP **05**, 143 (2017). https://doi.org/10.1007/JHEP05(2017)143 arXiv:1703.08505 [hep-ex]

48. J. Lees et al., BaBar Phys. Rev. D **85**, 112010 (2012). https://doi.org/10.1103/PhysRevD.85.112010 arXiv:1201.5897 [hep-ex]

49. S. Ropertz, C. Hanhart, B. Kubis, Eur. Phys. J. C **78**, 1000 (2018). https://doi.org/10.1140/epjc/s10052-018-6416-6 arXiv:1809.06867 [hep-ph]

50. D. Barberis et al., (WA102). Phys. Lett. B **453**, 305 (1999). https://doi.org/10.1016/S0370-2693(99)00365-2. arXiv:hep-ex/9903042

51. S. Uehara et al. (Belle), PTEP **013**, 123C01 (2013). https://doi.org/10.1093/ptep/ptt097. arXiv:1307.7457 [hep-ex]

52. K.T. Chao, X.-G. He, J.P. Ma, Eur. Phys. J. C **55**, 417 (2008). https://doi.org/10.1140/epjc/s10052-008-0606-6 arXiv:hep-ph/0512327

53. K.-T. Chao, X.-G. He, J.-P. Ma, Phys. Rev. Lett. **98**, 149103 (2007). https://doi.org/10.1103/PhysRevLett.98.149103 arXiv:0704.1061 [hep-ph]

54. M.S. Chanowitz, Phys. Rev. Lett. **98**, 149104 (2007). https://doi.org/10.1103/PhysRevLett.98.149104 arXiv:0704.1616 [hep-ph]

55. J.P. Lees et al., (BaBar), Phys. Rev. D **104**, 072002 (2021), https://doi.org/10.1103/PhysRevD.104.072002. arXiv:2106.05157 [hep-ex]

56. A. Rodas et al., JPAC Phys. Rev. Lett. **122**, 042002 (2019). https://doi.org/10.1103/PhysRevLett.122.042002 arXiv:1810.04171 [hep-ph]

57. A.V. Anisovich, C.A. Baker, C.J. Batty, D.V. Bugg, C. Hodd, H.C. Lu, V.A. Nikonov, A.V. Sarantsev, V.V. Sarantsev, B.S. Zou, Phys. Lett. B **491**, 47 (2000). https://doi.org/10.1016/S0370-2693(00)01018-2 arXiv:1109.0883 [hep-ex]

58. D.V. Bugg, Eur. Phys. J. C **36**, 161 (2004). https://doi.org/10.1140/epjc/s2004-01955-5 arXiv:hep-ph/0406292

59. A.V. Sarantsev, I. Denisenko, U. Thoma, E. Klempt, Phys. Lett. B **816**, 136227 (2021). https://doi.org/10.1016/j.physletb.2021.136227 arXiv:2103.09680 [hep-ph]

60. E. Klempt, Phys. Lett. B **820**, 136512 (2021). https://doi.org/10.1016/j.physletb.2021.136512 arXiv:2104.09922 [hep-ph]

61. E. Klempt, A.V. Sarantsev, arXiv:2112.04348 [hep-ph] (2021)

62. J.R. Peláez, A. Rodas, Eur. Phys. J. C **78**, 897 (2018). https://doi.org/10.1140/epjc/s10052-018-6296-9 arXiv:1807.04543 [hep-ph]

63. J. Peláez, A. Rodas, arXiv:2010.11222 [hep-ph] (2020)

64. R.A. Briceño, J.J. Dudek, R.G. Edwards, D.J. Wilson, Phys. Rev. D **97**, 054513 (2018). https://doi.org/10.1103/PhysRevD.97.054513 arXiv:1708.06667 [hep-lat]

65. R. Molina, D. Nicmorus, E. Oset, Phys. Rev. D **78**, 114018 (2008). https://doi.org/10.1103/PhysRevD.78.114018 arXiv:0809.2233 [hep-ph]

66. D. Gülmez, U.G. Meißner, J.A. Oller, Eur. Phys. J. C **77**, 460 (2017). https://doi.org/10.1140/epjc/s10052-017-5018-z arXiv:1611.00168 [hep-ph]

67. L.-S. Geng, R. Molina, E. Oset, Chin. Phys. C **41**, 124101 (2017). https://doi.org/10.1088/1674-1137/41/12/124101 arXiv:1612.07871 [nucl-th]

68. M.-L. Du, D. Gülmez, F.-K. Guo, U.-G. Meißner, Q. Wang, Eur. Phys. J. C **78**, 988 (2018). https://doi.org/10.1140/epjc/s10052-018-6475-8 arXiv:1808.09664 [hep-ph]

69. R. Molina, L.S. Geng, E. Oset, PTEP **2019**, 103B05 (2019). https://doi.org/10.1093/ptep/ptz109 arXiv:1903.04674 [hep-ph]

70. S. Descotes-Genon, B. Moussallam, Eur. Phys. J. C **48**, 553 (2006). https://doi.org/10.1140/epjc/s10052-006-0036-2 arXiv:hep-ph/0607133

71. M. Hoferichter, D.R. Phillips, C. Schat, Eur. Phys. J. C **71**, 1743 (2011). https://doi.org/10.1140/epjc/s10052-011-1743-x arXiv:1106.4147 [hep-ph]

72. C. Ditsche, M. Hoferichter, B. Kubis, U.G. Meißner, JHEP **06**, 043 (2012). https://doi.org/10.1007/JHEP06(2012)043 arXiv:1203.4758 [hep-ph]

73. J. Peláez, A. Rodas, Phys. Rev. Lett. **124**, 172001 (2020). https://doi.org/10.1103/PhysRevLett.124.172001 arXiv:2001.08153 [hep-ph]

74. P. Masjuan, J.J. Sanz-Cillero, Eur. Phys. J. C **73**, 2594 (2013). https://doi.org/10.1140/epjc/s10052-013-2594-4 arXiv:1306.6308 [hep-ph]

75. P. Masjuan, J. Ruiz de Elvira, J.J. Sanz-Cillero, Phys. Rev. D **90**, 097901 (2014). https://doi.org/10.1103/PhysRevD.90.097901 arXiv:1410.2397 [hep-ph]

76. I. Caprini, P. Masjuan, J. Ruiz de Elvira, J.J. Sanz-Cillero, Phys. Rev. D **93**, 076004 (2016). https://doi.org/10.1103/PhysRevD.93.076004 arXiv:1602.02062 [hep-ph]

77. J.R. Peláez, A. Rodas, J. Ruiz de Elvira, Eur. Phys. J. C **77**, 91 (2017). https://doi.org/10.1140/epjc/s10052-017-4668-1 arXiv:1612.07966 [hep-ph]

78. A. Švarc, M. Hadžimehmedović, H. Osmanović, J. Stahov, L. Tiator, R.L. Workman, Phys. Rev. C **89**, 065208 (2014). https://doi.org/10.1103/PhysRevC.89.065208 arXiv:1404.1544 [nucl-th]

79. R.-A. Tripolt, I. Haritan, J. Wambach, N. Moiseyev, Phys. Lett. B **774**, 411 (2017). https://doi.org/10.1016/j.physletb.2017.10.001 arXiv:1610.03252 [hep-ph]

80. R.-A. Tripolt, P. Gubler, M. Ulybyshev, L. Von Smekal, Comput. Phys. Commun. **237**, 129 (2019). https://doi.org/10.1016/j.cpc.2018.11.012 arXiv:1801.10348 [hep-ph]

81. D. Binosi, R.-A. Tripolt, Phys. Lett. B **801**, 135171 (2020). https://doi.org/10.1016/j.physletb.2019.135171 arXiv:1904.08172 [hep-ph]

82. D.V. Bugg, B.S. Zou, A.V. Sarantsev, Nucl. Phys. B **471**, 59 (1996). https://doi.org/10.1016/0550-3213(96)00166-6

83. R.S. Longacre et al., Phys. Lett. B **177**, 223 (1986). https://doi.org/10.1016/0370-2693(86)91061-0

84. P. A. Zyla *et al.* (Particle Data Group), PTEP **2020**, 083C01 (2020) https://doi.org/10.1093/ptep/ptaa104

85. M. Ablikim et al. (BESIII), Phys. Rev. D **92**, 052003 (2015), https://doi.org/10.1103/PhysRevD.92.052003. arXiv:1506.00546 [hep-ex]. [Erratum: Phys. Rev. D 93, no. 3, 039906 (2016)]

86. A. Jackura et al., (COMPASS and JPAC), Phys. Lett. B **779**, 464–472 (2018). https://doi.org/10.1016/j.physletb.2018.01.017. arXiv:1707.02848 [hep-ph]

87. B. Kopf, M. Albrecht, H. Koch, J. Pychy, X. Qin, U. Wiedner, arXiv:2008.11566 [hep-ph] (2020)

88. R.M. Baltrusaitis et al., (MARK-III), Phys. Rev. D **33**, 1222 (1986). https://doi.org/10.1103/PhysRevD.33.1222

89. D. Bisello et al., (DM2), Phys. Rev. D **39**, 701 (1989). https://doi.org/10.1103/PhysRevD.39.701

90. J. Bai, et al., (BES), Phys. Lett. B **472**, 207 (2000). https://doi.org/10.1016/S0370-2693(99)01393-3. arXiv:hep-ex/9909040

91. W.H. Press, S.A. Teukolsky, W.T. Vetterling, B.P. Flannery, *Numerical Recipes 3rd Edition: The Art of Scientific Computing*, 3rd edn. (Cambridge University Press, New York, 2007)

92. B. Efron and R. Tibshirani, *An Introduction to the Bootstrap, Chapman & Hall/CRC Monographs on Statistics and Applied Probability* (Taylor & Francis, 1994). https://www.crcpress.com/An-Introduction-to-the-Bootstrap/Efron-Tibshirani/p/book/9780412042317

93. J. Landay, M. Döring, C. Fernández-Ramírez, B. Hu, R. Molina, Phys. Rev. C **95**, 015203 (2017). https://doi.org/10.1103/PhysRevC.95.015203 arXiv:1610.07547 [nucl-th]

94. K.J. Sebastian, H. Grotch, F.L. Ridener, Phys. Rev. D **45**, 3163 (1992). https://doi.org/10.1103/PhysRevD.45.3163

95. R. Kaminski, L. Lesniak, K. Rybicki, Z. Phys. C **74**, 79 (1997). https://doi.org/10.1007/s002880050372 arXiv:hep-ph/9606362

96. J.R. Batley et al., (NA48-2), Eur. Phys. J. C **70**, 635 (2010). https://doi.org/10.1140/epjc/s10052-010-1480-6

97. J. Pelaez, A. Rodas, J. Ruiz De Elvira, Eur. Phys. J. C **79**, 1008 (2019). https://doi.org/10.1140/epjc/s10052-019-7509-6 arXiv:1907.13162 [hep-ph]

98. F. Niecknig, B. Kubis, S.P. Schneider, Eur. Phys. J. C **72**, 2014 (2012). https://doi.org/10.1140/epjc/s10052-012-2014-1 arXiv:1203.2501 [hep-ph]

99. L. Gan, B. Kubis, E. Passemar, S. Tulin, arXiv:2007.00664 [hep-ph] (2020)

100. M. Albaladejo, I. Danilkin, S. Gonzàlez-Solís, D. Winney, C. Fernández-Ramírez, A. HillerBlin, V. Mathieu, M. Mikhasenko, A. Pilloni, A. Szczepaniak, Eur. Phys. J. C **80**, 1107 (2020). https://doi.org/10.1140/epjc/s10052-020-08576-6 arXiv:2006.01058 [hep-ph]

101. K.M. Watson, Phys. Rev. **88**, 1163 (1952). https://doi.org/10.1103/PhysRev.88.1163

102. Ł Bibrzycki, C. Fernández-Ramírez, V. Mathieu, M. Mikhasenko, M. Albaladejo, A.N. Hiller Blin, A. Pilloni, A.P. Szczepaniak, Eur. Phys. J. C **81**, 647 (2021). https://doi.org/10.1140/epjc/s10052-021-09420-1

103. E. Barrelet, Nuovo Cim. A **8**, 331 (1972). https://doi.org/10.1007/BF02732655

104. G.F. Chew, S. Mandelstam, Phys. Rev. **119**, 467 (1960). https://doi.org/10.1103/PhysRev.119.467

105. J.D. Bjorken, Phys. Rev. Lett. **4**, 473 (1960). https://doi.org/10.1103/PhysRevLett.4.473

106. I.J.R. Aitchison, Nucl. Phys. A **189**, 417 (1972). https://doi.org/10.1016/0375-9474(72)90305-3

107. J.A. Oller, E. Oset, J.R. Peláez, Phys. Rev. D **59**, 074001 (1999). https://doi.org/10.1103/PhysRevD.59.074001. arXiv:hep-ph/9804209 [Erratum: Phys.Rev.D 60, 099906 (1999), Erratum: Phys.Rev.D 75, 099903 (2007)],

108. L. Castillejo, R.H. Dalitz, F.J. Dyson, Phys. Rev. **101**, 453 (1956). https://doi.org/10.1103/PhysRev.101.453

109. I. Bedlinskiy et al., (CLAS), Phys. Rev. C **90**, 025205 (2014). https://doi.org/10.1103/PhysRevC.90.039901. arXiv:1405.0988 [nucl-ex] [Addendum: Phys.Rev.C 90, 039901 (2014)]

110. F. James, M. Roos, Comput. Phys. Commun. **10**, 343 (1975). https://doi.org/10.1016/0010-4655(75)90039-9

111. T. Schlüter, The $\pi^-\eta$ and $\pi^-\eta'$ systems in exclusive 190 GeV $\pi^- p$ reactions at COMPASS. Ph.D. thesis, Munich U. (2012)

112. M. Mikhasenko, A. Pilloni, M. Albaladejo, C. Fernández-Ramírez, A. Jackura, V. Mathieu, J. Nys, A. Rodas, B. Ketzer, A.P. Szczepaniak, (JPAC), Phys. Rev. D **98**, 096021 (2018). https://doi.org/10.1103/PhysRevD.98.096021. arXiv:1810.00016 [hep-ph]

113. R.A. Briceño, J.J. Dudek, L. Leskovec, Phys. Rev. D **104**, 054509 (2021). https://doi.org/10.1103/PhysRevD.104.054509 arXiv:2105.02017 [hep-lat]

114. A. Pilloni, C. Fernández-Ramírez, A. Jackura, V. Mathieu, M. Mikhasenko, J. Nys, A.P. Szczepaniak, (JPAC), Phys. Lett. B **772**, 200 (2017). https://doi.org/10.1016/j.physletb.2017.06.030. arXiv:1612.06490 [hep-ph]

115. R. Molina, J. Ruiz de Elvira, JHEP **11**, 017 (2020). https://doi.org/10.1007/JHEP11(2020)017 arXiv:2005.13584 [hep-lat]

116. M. Niehus, M. Hoferichter, B. Kubis, J. Ruiz de Elvira, Phys. Rev. Lett. **126**, 102002 (2021). https://doi.org/10.1103/PhysRevLett.126.102002 arXiv:2009.04479 [hep-ph]

117. C. Fernández-Ramírez, A. Pilloni, M. Albaladejo, A. Jackura, V. Mathieu, M. Mikhasenko, J.A. Silva-Castro, A.P. Szczepaniak (JPAC), Phys. Rev. Lett. **123**, 092001 (2019). https://doi.org/10.1103/PhysRevLett.123.092001. arXiv:1904.10021 [hep-ph]

118. A.N. Hiller Blin, C. Fernández-Ramírez, A. Jackura, V. Mathieu, V.I. Mokeev, A. Pilloni, A.P. Szczepaniak, Phys. Rev. D **94**, 034002 (2016). https://doi.org/10.1103/PhysRevD.94.034002 arXiv:1606.08912 [hep-ph]